Enhanced retinal vasculature imaging with a rapidly configurable aperture

KAITLYN A. SAPOZNIK[1,*], TING LUO[1], ALBERTO DE CASTRO[1], LUCIE SAWIDES[1], RAYMOND L. WARNER[1], AND STEPHEN A. BURNS[1]

[1]*School of Optometry, Indiana University, 800 E. Atwater Avenue, Bloomington, IN 47405,*
*ksapozni@indiana.edu

Abstract: In adaptive optics scanning laser ophthalmoscope (AOSLO) systems, capturing the multiply scattered light can increase the contrast of the retinal microvasculature structure, cone inner segments, and retinal ganglion cells. Current systems generally use either a split detector or offset aperture approach to collect this light. We tested the ability of a spatial light modulator (SLM) as a rapidly configurable aperture to use more complex shapes to enhance contrast of retinal structure. Particularly, we varied the orientation of a split detector aperture and explored the use of a more complex shape, the half annulus, to enhance the contrast of the retinal vasculature. We used the new approach to investigate the influence of scattering distance and orientation on vascular imaging.

References and links (see Section 4)

1. R. H. Webb, G. W. Hughes, and F. C. Delori, "Confocal scanning laser ophthalmoscope," Applied optics **26**, 1492-1499 (1987).
2. A. Elsner, M. Miura, S. Burns, E. Beausencourt, C. Kunze, L. Kelley, J. Walker, G. Wing, P. Raskauskas, D. Fletcher, Q. Zhou, and A. Dreher, "Multiply scattered light tomography and confocal imaging: detecting neovascularization in age-related macular degeneration," Optics express **7**, 95-106 (2000).
3. A. E. Elsner, S. A. Burns, J. J. Weiter, and F. C. Delori, "Infrared imaging of sub-retinal structures in the human ocular fundus," Vision research **36**, 191-205 (1996).
4. T. Y. Chui, D. A. Vannasdale, and S. A. Burns, "The use of forward scatter to improve retinal vascular imaging with an adaptive optics scanning laser ophthalmoscope," Biomedical optics express **3**, 2537-2549 (2012).
5. D. Scoles, Y. N. Sulai, C. S. Langlo, G. A. Fishman, C. A. Curcio, J. Carroll, and A. Dubra, "In vivo imaging of human cone photoreceptor inner segments," Investigative ophthalmology & visual science **55**, 4244-4251 (2014).
6. S. A. Burns, A. E. Elsner, M. B. Mellem-Kairala, and R. B. Simmons, "Improved contrast of subretinal structures using polarization analysis," Investigative ophthalmology & visual science **44**, 4061-4068 (2003).
7. S. A. Burns, A. E. Elsner, T. Y. Chui, D. A. Vannasdale, Jr., C. A. Clark, T. J. Gast, V. E. Malinovsky, and A. D. Phan, "In vivo adaptive optics microvascular imaging in diabetic patients without clinically severe diabetic retinopathy," Biomedical optics express **5**, 961-974 (2014).
8. J. G. Hillard, T. J. Gast, T. Y. Chui, D. Sapir, and S. A. Burns, "Retinal Arterioles in Hypo-, Normo-, and Hypertensive Subjects Measured Using Adaptive Optics," Translational vision science & technology **5**, 16 (2016).
9. T. Y. Chui, T. J. Gast, and S. A. Burns, "Imaging of vascular wall fine structure in the human retina using adaptive optics scanning laser ophthalmoscopy," Investigative ophthalmology & visual science **54**, 7115-7124 (2013).
10. T. Y. Chui, M. Dubow, A. Pinhas, N. Shah, A. Gan, R. Weitz, Y. N. Sulai, A. Dubra, and R. B. Rosen, "Comparison of adaptive optics scanning light ophthalmoscopic fluorescein angiography and offset pinhole imaging," Biomedical optics express **5**, 1173-1189 (2014).
11. A. de Castro, G. Huang, L. Sawides, T. Luo, and S. A. Burns, "Rapid high resolution imaging with a dual-channel scanning technique," Optics letters **41**, 1881-1884 (2016).
12. Y. N. Sulai, D. Scoles, Z. Harvey, and A. Dubra, "Visualization of retinal vascular structure and perfusion with a nonconfocal adaptive optics scanning light ophthalmoscope," Journal of the Optical Society of America. A, Optics, image science, and vision **31**, 569-579 (2014).
13. L. W. Sun, R. D. Johnson, V. Williams, P. Summerfelt, A. Dubra, D. V. Weinberg, K. E. Stepien, G. A. Fishman, and J. Carroll, "Multimodal Imaging of Photoreceptor Structure in Choroideremia," PloS one **11**, e0167526 (2016).

14. B. J. King, K. A. Sapoznik, A. E. Elsner, T. J. Gast, J. A. Papay, C. A. Clark, and S. A. Burns, "SD-OCT and Adaptive Optics Imaging of Outer Retinal Tubulation," Optometry and vision science : official publication of the American Academy of Optometry **94**, 411-422 (2017).
15. M. A. Abozaid, C. S. Langlo, A. M. Dubis, M. Michaelides, S. Tarima, and J. Carroll, "Reliability and Repeatability of Cone Density Measurements in Patients with Congenital Achromatopsia," Advances in experimental medicine and biology **854**, 277-283 (2016).
16. C. S. Langlo, L. R. Erker, M. Parker, E. J. Patterson, B. P. Higgins, P. Summerfelt, M. M. Razeen, F. T. Collison, G. A. Fishman, C. N. Kay, J. Zhang, R. G. Weleber, P. Yang, M. E. Pennesi, B. L. Lam, J. D. Chulay, A. Dubra, W. W. Hauswirth, D. J. Wilson, J. Carroll, and A.-s. group, "Repeatability and Longitudinal Assessment of Foveal Cone Structure in Cngb3-Associated Achromatopsia," Retina **37**, 1956-1966 (2017).
17. C. S. Langlo, E. J. Patterson, B. P. Higgins, P. Summerfelt, M. M. Razeen, L. R. Erker, M. Parker, F. T. Collison, G. A. Fishman, C. N. Kay, J. Zhang, R. G. Weleber, P. Yang, D. J. Wilson, M. E. Pennesi, B. L. Lam, J. Chiang, J. D. Chulay, A. Dubra, W. W. Hauswirth, J. Carroll, and A.-S. Group, "Residual Foveal Cone Structure in CNGB3-Associated Achromatopsia," Investigative ophthalmology & visual science **57**, 3984-3995 (2016).
18. K. M. Litts, R. F. Cooper, J. L. Duncan, and J. Carroll, "Photoreceptor-Based Biomarkers in AOSLO Retinal Imaging," Investigative ophthalmology & visual science **58**, BIO255-BIO267 (2017).
19. E. A. Rossi, C. E. Granger, R. Sharma, Q. Yang, K. Saito, C. Schwarz, S. Walters, K. Nozato, J. Zhang, T. Kawakami, W. Fischer, L. R. Latchney, J. J. Hunter, M. M. Chung, and D. R. Williams, "Imaging individual neurons in the retinal ganglion cell layer of the living eye," Proceedings of the National Academy of Sciences of the United States of America **114**, 586-591 (2017).
20. S. A. Burns, R. Tumbar, A. E. Elsner, D. Ferguson, and D. X. Hammer, "Large-field-of-view, modular, stabilized, adaptive-optics-based scanning laser ophthalmoscope," Journal of the Optical Society of America. A, Optics, image science, and vision **24**, 1313-1326 (2007).
21. R. D. Ferguson, Z. Zhong, D. X. Hammer, M. Mujat, A. H. Patel, C. Deng, W. Zou, and S. A. Burns, "Adaptive optics scanning laser ophthalmoscope with integrated wide-field retinal imaging and tracking," Journal of the Optical Society of America. A, Optics, image science, and vision **27**, A265-277 (2010).
22. W. Zou, X. Qi, and S. A. Burns, "Woofer-tweeter adaptive optics scanning laser ophthalmoscopic imaging based on Lagrange-multiplier damped least-squares algorithm," Biomedical optics express **2**, 1986-2004 (2011).
23. W. Zou, X. Qi, and S. A. Burns, "Wavefront-aberration sorting and correction for a dual-deformable-mirror adaptive-optics system," Optics letters **33**, 2602-2604 (2008).
24. T. Luo, T. J. Gast, T. J. Vermeer, and S. A. Burns, "Retinal Vascular Branching in Healthy and Diabetic Subjects," Investigative ophthalmology & visual science **58**, 2685-2694 (2017).
25. G. Huang, Z. Zhong, W. Zou, and S. A. Burns, "Lucky averaging: quality improvement of adaptive optics scanning laser ophthalmoscope images," Optics letters **36**, 3786-3788 (2011).
26. K. Hueck, A. Mazurenko, N. Luick, T. Lompe, and H. Moritz, "Note: Suppression of kHz-frequency switching noise in digital micro-mirror devices," The Review of scientific instruments **88**, 016103 (2017).

1. Introduction

When illuminated, retinal structures may directly scatter light back through the system pupil, and be captured directly by the imaging system, or may scatter light in other directions [1]. If an image is formed from these other portions of light that have undergone additional scattering and subsequently exit the pupil, the images are generically referred to as indirect or multiply scattered light images [1-3]. While most images are actually combinations of singly and multiply scattered light, confocal images emphasize the singly scattering light whereas multiply scattered light images reveal information about structures that may otherwise be nearly transparent and not readily imaged using confocal imaging [2-6].

In current adaptive optics scanning laser ophthalmoscope (AOSLO) systems, two main approaches are utilized to capture multiply scattered light: 1) an offset aperture displaced from the center of the point spread function (PSF) [4] and 2) a split detector in which the center of the PSF is removed and light in two directions is collected [5]. Chui et al. [4] first utilized multiply scattered light imaging within an AOSLO by using an offset aperture to improve imaging of vascular wall structures that were not readily observed in confocal imaging. Pathological changes to the vessel wall structure are of particular interest in subjects with diabetes and hypertension and have been observed with this technique [7, 8]. Furthermore, this approach has proven useful in characterizing the murals cells of the retinal vasculature [9]; to detect subclinical vascular and cystic changes in subjects with diabetes [7]; characterize wall-to-lumen ratios (WLR) in normo-, hypo-, and hypertensive subjects [8]; provide perfusion maps comparable to AOSLO fluorescein angiography [10]; and detect

erythrocytes in small capillaries to compute blood flow velocity [11]. Similar to the offset aperture, split detection systems have proven useful in imaging the retinal microvasculature producing similar results to those of an offset aperture [12] and the detection of cone inner segments [5]. Both split detection and offset aperture variations of multiply scattered light AOSLO imaging enable the inner segments to be visualized and this has proven useful in improving our understanding of photoreceptor structure in several retinal diseases affecting the photoreceptors. In particular, indirect imaging of the cones provides additive information regarding the integrity of photoreceptors whose outer segments are not functioning or oriented properly in choroideremia [13], outer retinal tubulation [14], and achromatopsia[15-17]. The use of multiply scattered light photoreceptor imaging is expanding rapidly and is currently being investigated as a potential biomarker for therapeutic interventions in some hereditary retinal degenerations [18].

Additionally, there has been a focus of the adaptive optics community on using multiply scattered light imaging to improve visibility of other retinal cells not readily imaged with confocal imaging approaches. Rossi et al. [19] recently demonstrated the ability of AOSLO systems to image retinal ganglion cell (RGC) layer neurons in both monkeys and humans by capturing images of the same retinal region with multiple offset aperture configurations. Contrast of the RGC layer neurons could then be further enhanced by combining contrast across scattering directions.

The light captured in multiply scattered light imaging arises from both scattering and refraction of the incident light, and is also dependent on the path of light until the next scattering event. Given the heterogeneity of sizes and scattering distances, more flexible approaches to collecting multiply scattered light should enable improvement of the contrast of structures of interest. In this study, we used a spatial light modulator (SLM) in a retinal plane of our AOSLO to serve as an aperture to image multiply scattered light. By programming specific shapes onto the SLM, non-standard aperture configurations can be chosen and manipulated dynamically. In the current work we implement such a system and investigate its applicability to imaging the retinal microvasculature. For this work we concentrate on testing the utility of using an SLM to improve understanding of light tissue interactions that control the contrast of imaging the inner retina.

2. Methods

2.1 Subjects

Nine eyes from nine normal subjects (23-94 years of age, mean ± SD, 26.6±3.4, 6 males and 3 females) with no retinal pathology and one eye from one hypertensive (HTN) subject (31 year old female) were imaged. Informed consent was obtained prior to imaging in all subjects. The research was approved by the Indiana University Institutional Review Board and complied with the tenets of the Declaration of Helsinki.

2.2 AOSLO System

For this work we used a new AOSLO system similar to the Indiana AOSLO previously described [20-22]. The current AOSLO is a dual-channel system that combines a Shack Hartmann (SH) wavefront sensor with two deformable mirrors in a woofer-tweeter design [22, 23] that corrects for optical aberrations over a wide range of refractive errors. Two simultaneous imaging channels (769 nm and the other at 840 nm) derived from a supercontinuum laser (Fianium, NKT Photonics, Birkerod, Denmark), are used to scan the retina. Each detection channel contains retinal conjugate apertures that can be manually configured at the retinal plane and the light from the retina is detected using avalanche photodiodes (APD, Pacer C30659-90, together with custom amplifier and temperature controller). For both channels, the Airy disk diameter (ADD) at the plane of the confocal pinhole was 50 µm. In the first imaging channel (769 nm) light was imaged onto a 2 Airy

disk diameter (ADD) confocal pinhole. Light passing through the pinhole from the center of the PSF formed the confocal image. The surround of the pinhole was a reflective metallic surface. Light reflecting from this surface, from the outer portions of the PSF, was refocused onto the SLM as described below. In channel 2 (840 nm), a 10 ADD pinhole was displaced 6 ADD superiorly with respect to the retina to collect multiply scattered light images as previously described [4]. Channel 2 was intentionally spatially offset from Channel 1 [11].

Figure 1 incorporates a Zemax drawing (Zemax, LLC, Kirkland, WA, USA) in a schematic diagram of the channel 1 detection scheme. Light reflected from the surface of the confocal pinhole contains most of the multiply scattered light (the outer portions of the PSF). To capture as wide an extent of the PSF tails as possible we used a reflective stainless steel aperture (Edmund Optics, Barrington, NJ, USA) where the reflective surface was 190 ADD wide. This reflected light is re-imaged by two lenses at 1:1 magnification onto a second retinal conjugate plane where an SLM is placed (DLP6500FLQ, Texas Instruments, Dallas, TX). This enables the SLM to serve as an additional aperture at a retinal conjugate plane for collecting multiply scattered light.
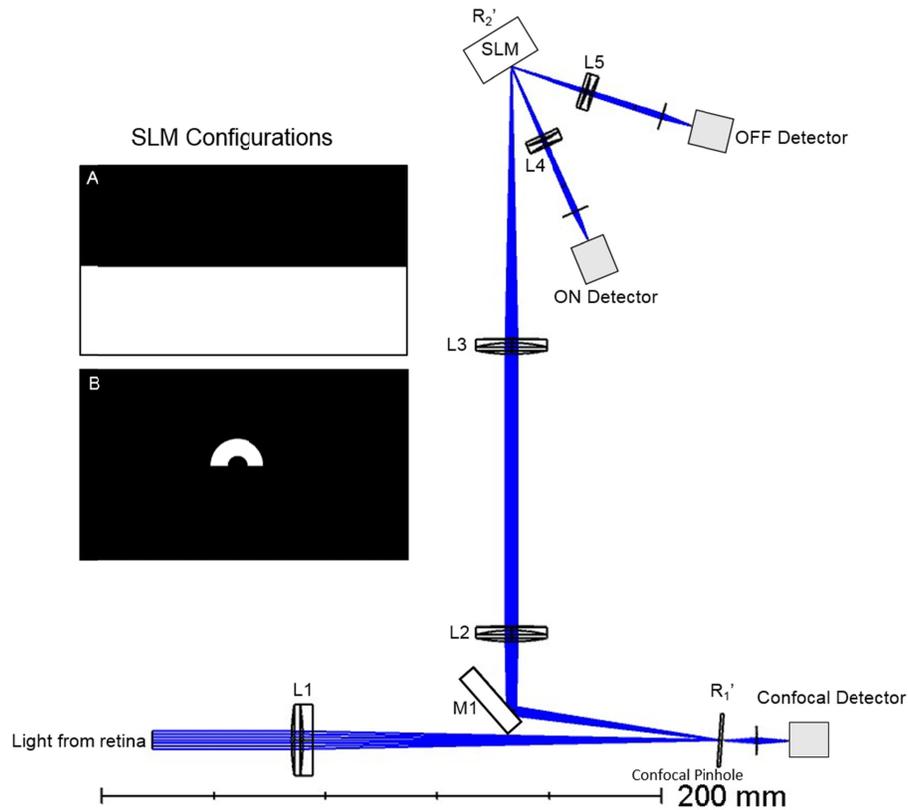

Fig. 1. Zemax schematic of channel 1 detection. Light from the retina passes through a confocal pinhole at the first retinal conjugate plane (R1') to produce a confocal image. The PSF surround is reflected from the pinhole surface and re-imaged to a second retinal conjugate plane (R2'). A series of lenses (L2-L3) are utilized to maintain a 1:1 magnification ratio at the SLM after the reflected light passes through a turning mirror (M1). At R2' light is reflected to either the ON or OFF detector by an SLM (micromirror array) acting as a programmable aperture. A. Example of a split detector configuration on the array (ON = white, OFF = black). B. Example of a half annulus configuration on the array.

The SLM consists of a 1920x1080 micromirror array. The micromirror array has a 7.56 µm (0.15 ADD) pitch and a 2.55 µs micromirror crossover time. The micromirrors have two tilt angles, $\pm12^0$, with respect to the flat state and we term the positive tilt direction as the "ON" state while the negative tilt direction is termed the "OFF" state. The micromirrors are arranged in a diamond configuration and tilt around the diagonal. We oriented the chip so the axis of rotation was vertical, allowing us to keep our detectors in a horizontal plane. The fill factor of this SLM is 92% and the diffraction efficiency specification is 86%. We did not use the chip designed for near IR, since in general the amount of light available under our conditions of interest is much higher than available through the confocal aperture. This allowed us to work with an array that we estimate to be about 60% efficient overall. The impact of diffraction from the SLM was larger in the off state, due to the angle on incidence on the mirrors, but lenses L4 and L5 had sufficiently large apertures to collect all major diffraction orders. By providing the SLM control mechanism with a binary map, virtually any pattern can be programmed onto the SLM. To generate the pattern onto the SLM, custom MATLAB software (Mathworks, Natick, MA, USA) generated the aperture shape and communicated with the SLM controller via USB. Thus, for example, to enable a split detection aperture commonly used by others [5, 12], we can program half of the array to the "ON" state and other half to the "OFF" state (Fig. 1A). Likewise, in this study, we also utilized a related shape, a half annulus, where the half annulus shape is programmed to the "ON" state, while the remainder of the mirrors are in the "OFF" state (Fig 1B). Light from both the "ON" and "OFF" states are each then focused onto separate APD detectors by a pair
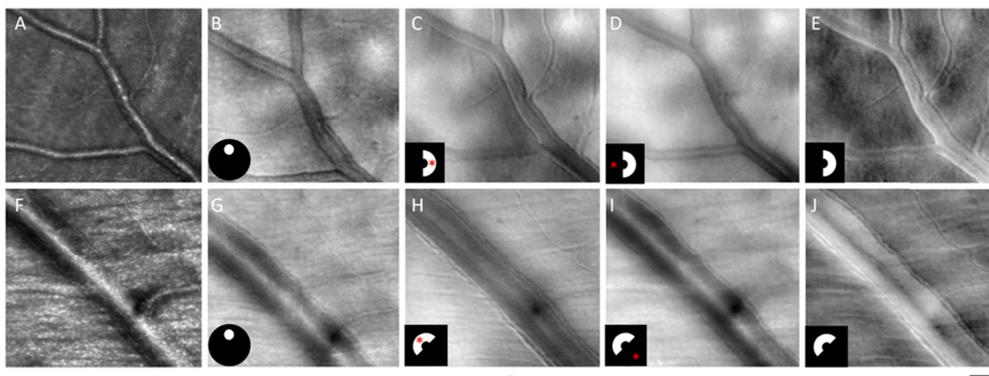

Fig. 2. Simultaneously acquired images on a venule and arteriole in a normal 34 year old male. Venule images (A-E). Arteriole images (F-J). A and F. Confocal images from the first channel (2 ADD centered aperture). B and G. Offset aperture images (10 ADD displaced aperture) from the second channel. C, D, and E. ON, OFF and ratio multiply scattered light images of the venule obtained with a split annulus orientated at 270° with an inner radius of 5.3 ADD and outer radius of 22.7 ADD. H, I and J. ON, OFF and ratio multiply scattered light images obtained with a half annulus oriented at 45° and with an inner radius of 8.3 ADD (H) and an outer radius of 22.7 ADD. Excellent wall contrast of both the arteriole (H and J) and venule (C and E) is generated with the split annulus apertures. The insets depict the aperture configuration at the center of the SLM with the red asterisk indicating the portion of the array generating the image. Scale bar = 50µm.

of lenses. In this way we generate 3 simultaneous images (Fig. 2) from channel 1:1) confocal image, 2) multiply scattered light image from the "ON" state of the SLM, and 3) another multiply scattered light imaged from the "OFF" state of the SLM. From channel 2 we generate 1 multiply scattered light image with a fixed offset aperture.

2.3 AOSLO Imaging session

Each subject was dilated with 0.5% or 1% tropicamide ophthalmic solution and axial lengths were measured (IOL Master; Version 5; Carl Zeiss Meditec, Dublin, CA, USA) prior to the

imaging session. In each imaging session we measured changes in contrast of one or more features for a series of aperture conditions. For this work we concentrated primarily on smaller retinal arterioles and venules between 20-50μm since they have different wall structures and quantification of changes to small vessels are important for understanding the impact of both diabetes [7, 24] and hypertension [8]. To limit the number of shapes used we concentrated on a subset of variations of two simple shape configurations that provided both flexibility to investigate scattering distances and orientations and were likely to be sensitive to a range of retinal features; a split detector (Fig. 1A) and half annulus (Fig. 1B).

In each subject 2-4 ROIs were selected in a single imaging session. At each ROI, the system was carefully focused in the plane of the feature since all imaging modes are very sensitive to best focus. For the non-confocal modes this is presumably because contrast of small, high spatial frequency targets is dependent on the size of the scanning beam. At each ROI, either a 1.2^0 x 1.3^0 or 2^0 x 1.8^0 imaging field captured 2-4 videos of 100 frames (30 frames/second) with each programmed aperture variation. Between 4-12 different aperture variations were used at each ROI dependent on what programmed feature of the aperture was systematically varied. For the split detection configuration we concentrated on the orientation of the split between the "ON" and "OFF" detectors. For all subjects and all regions of interest (ROI's) splits were oriented at 0^0 or 90^0 with respect to the retina. For the half annulus we varied three parameters; 1) inner radius, 2) outer radius, and 3) the angle of orientation of the half annulus (axis of where it is halved).

To measure the scattering distance of retinal features, in 3 subjects, we began with a 10 ADD inner radius and 20 ADD outer radius and increased inner and outer radii together in 5 ADD increments until a half annulus ending with a 25 ADD inner radius and a 35 ADD outer radius. The half annulus orientation was held constant at 270^0 with respect to the retina.

To measure variations in scattering at smaller angular distances, in 9 subjects, the outer radius was held constant at 22.7 ADD while the inner radius was varied between 2.3 and 11.3 ADD in 1.5 ADD increments. The half annulus orientation was held constant at 270^0 with respect to the retina.

To measure the impact of scattering direction, in 9 subjects the inner and outer radii of a half annulus were held constant at 8.3 and 23.7 ADD while the orientation of the half annulus was rotated in 45^0 increments from 0^0 to 360^0 with respect to the retina.

2.4 Image Processing

After the imaging session, videos were corrected for sinusoidal distortions, aligned, and averaged, generating both standard averages and optimized averages [25] using custom Matlab programs.

The SLM utilized did not allow us complete control of mirror timing. To avoid mirror overheating in some applications the SLM manufacturer hard codes brief "flips" of the mirrors in the control system. These flips create high contrast black and white lines throughout the image, representing a few percent of each image. As the images generated from the SLM have low contrast, we removed these lines by computing the z-score of each pixel across all image frames, and removed all pixels with values outside 2 standard deviations from the mean or approximately 5% of the pixels. The resulting images were typically free of artifact from these mirror resets. Because alignment is performed on the confocal images, and these necessarily have identical eye movement components to the images from the SLM channels, this suffices to remove the impact of eye movements and SLM artifacts.

From the resulting "on" and "off" images we also calculated a contrast image by normalizing the difference of the two images by the sum similar to computations typically performed using a split detector configuration (Fig. 2. E and J) [5].

3. Results

3.1 SLM performance as an aperture

When placed at a retinal conjugate plane, an SLM can effectively be used as a configurable aperture. The SLM produces images of comparable quality to those generated by both our
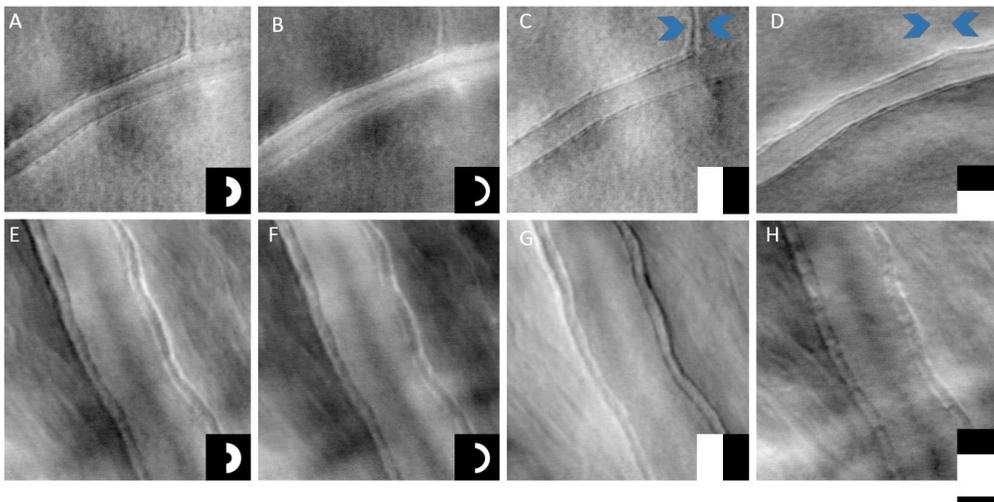

Fig. 3. Arteriole ratio images with different apertures. Small arteriole in a healthy 34 year old (A-D). Large arteriole in a hypertensive 31 year old (E-H). Mural cell contrast in the small arteriole is higher with a smaller inner radius (A, 3.8 ADD vs. B, 11.3 ADD) but not for the larger arteriole (E and F) for a fixed outer radius of 22.7 ADD. Orthogonal split detector orientation of a small (C and D) and large (G and H) arteriole. When the split detector is roughly orthogonal to the cell walls (C and H), the contrast of the mural cells is higher, whereas, when the split is roughly parallel to the wall itself, the contrast of the wall border is higher (D and G). Contrast of the small vessel branch (C and D, blue arrowheads) is highly dependent on the orientation of the split detector. Scale bar = 50μm.

standard confocal and offset aperture images (Fig. 2) although specific image features depended systematically on details of the programmable aperture used. Multiple aperture configurations could be rapidly generated and loaded onto the SLM allowing multiple views of the same feature to be obtained within an imaging session (Fig. 2-5). For the current study, within one imaging session lasting between 45-60 minutes, 4-12 aperture configurations were utilized for up to 4 ROIs. In general, the "OFF" detector had larger signals and lower contrast than the "ON" detector, other than for the split detector configurations (Fig. 2C vs. Fig. 2D and Fig. 2H vs. Fig. 2I). This occurred presumably due to the inclusion of a much larger proportion of the extended PSF being directed to the "OFF" detector than the ON" (Fig. 1), and the fact that it included a much wider range of angles and distances.

3.2 Scattering distance and direction

The retina scatters light in various directions and angles depending on the properties of the tissue and the local anatomy. For blood vessels the contrast of the vessel wall was improved with multiply scattered light imaging generated with the half annulus aperture, as opposed to the directly reflected light captured in the confocal image (Fig. 2A vs. Fig. 2C,E and Fig. 2F vs. Fig. 2H,J). Additionally, the contrast of the vessel walls is also improved in comparison to the standard offset aperture images (Fig. 2B and Fig. 2G) [4]. This increased contrast, as discussed below, is dependent on the characteristics of the aperture used for detection.

Varying the inner radius of the half annulus had an impact on contrast of the fine details of the vessel wall structure presumed to be mural cells [9]. For example, the contrast of the mural cells in smaller arterioles improved with the small to moderate inner radii tested (2.3-8.3 ADD) compared to imaging with a larger inner radii (Fig. 3A vs. Fig. 3B; 6.4% vs. 4.9%

Michelson contrast). At larger inner radii, scattering from the moving red blood cell column contributed more to vessel contrast (Fig. 3B). While we only imaged 5 larger vessels in this study, the walls were always visible and as a result the size of the inner radius did not have as great an impact. This is apparent in images of a larger arteriole in a hypertensive subject with thickened walls (Fig. 3E vs. Fig. 3F). For venules, where vascular walls are thin and usually difficult to image, small to moderate inner radii also improved the contrast (Fig. 2C-E). In general, vessel wall contrast continued to decrease at larger distances dropping to near zero beyond 30 ADD when both the inner and outer radii were increased (Fig. 4). However, for these larger distances scatter from the moving red blood cells predominated the images (Fig. 4).The contrast of structures also depended on the orientation of the aperture chosen. The impact of orientation was qualitatively similar for both the split detector (Fig. 3) and the half annulus (Fig. 5). Depending on orientation, the split detector may highlight fine vessel wall structure (Fig. 3C and Fig. 3H) or increase contrast of the wall edges compared to the surrounding retina (Fig. 3C vs. Fig. 3D; 20% vs. 35% Michelson contrast). The split detector orientation is also more sensitive to the contrast of the entire vessel structures. For example, when a small (13 µm) vessel branch is oriented parallel to the split, the contrast of the branch to the surrounding retina is high (Fig. 3C, blue arrowheads) compared to when the branch is orthogonal to the split and the contrast between it and the surrounding retina decreased to immeasurably low values (Fig. 3D, blue arrowheads). The half annulus, however, generally produces higher contrast for small features and did not show as strong an angular dependence

for entire structures. Instead, individual murals cells of the vessel walls oriented orthogonal to the aperture had the highest contrast but there was not as large a reduction in contrast between the surrounding retina and the vessel walls (Fig. 5). The half annulus also revealed a cellular array similar to that previously described [12, 19] just below the nerve fiber layer. While the array is evident in many of the split detector images (Fig. 2), the half annulus seemed more sensitive to enhancing the contrast of these presumed retinal ganglion cell (RGC) layer neurons [19]. This array often followed the orientation of the overlying nerve fiber layer bundles (Fig. 5).

4. Discussion

4.1 Improved efficiency

Multiply scattered light imaging in AOSLO systems, whether via split detection or offset aperture methods, has provided increased ability to image and interpret retinal vessel structure in normal eyes and changes to these structures arising from disease processes [4, 7-10, 12]. While systematically controlling the aperture direction and displacement has been shown to be beneficial[4], previous implementations required aperture parameters to be manipulated via electronic motor or manually, which can be time consuming and limit the number of scattered light images that can be collected. For example, Chui et al. [4] showed that when the direction of offset of an offset aperture is orthogonal to the orientation of the blood vessel, the contrast
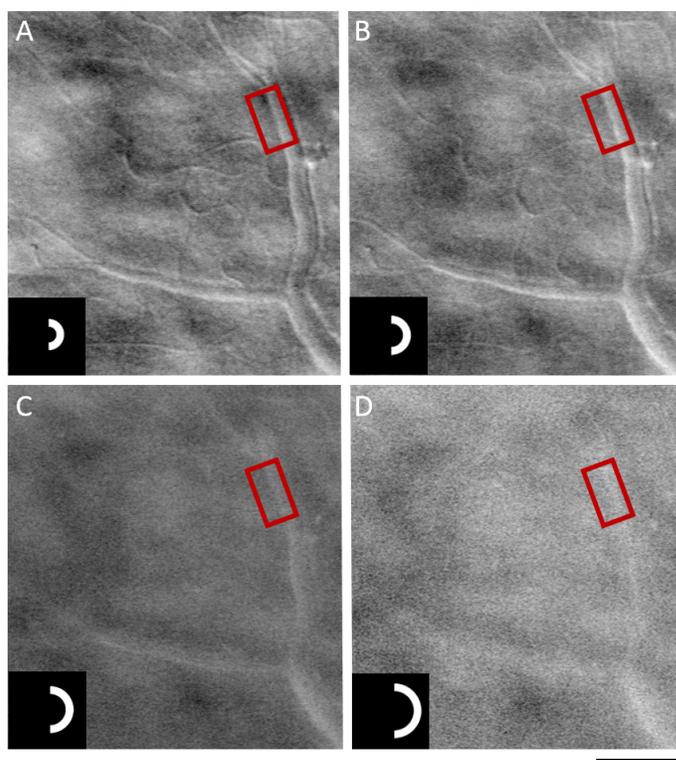

Fig. 4. Wall contrast depends on distance from the center of the PSF with a half annulus oriented roughly parallel to the vessel. Contrast was measured between the vessel wall and surrounding retina by integrating intensity values parallel to the vessel and averaging along roughly 70 μm (red box). As the inner radius increased from 10 ADD (A) to 25 ADD (D) in 5 ADD increments, contrast decreased from 21.3% (A), 13.5% (B), 10.6% (C), to 2.4% (D). The outer radius was maintained at 5 ADD larger than the inner radius. Scale bar = 100 μm.

of the mural features of only the wall orthogonal to the direction of offset is maximized. Thus, when an offset aperture is maintained in a fixed position, potentially beneficial information from that vessel of the light scattered elsewhere may be lost. Likewise, split detectors are also generally left in a fixed orientation and entire structures may be lost (Fig. 3D). Using an SLM as a rapidly configurable aperture enables the orientation and displacement of a particular shape to be easily configured, improving the characterization of the feature of interest by capturing the scattered light at different distances and directions in an efficient manner, that for predetermined shapes and orientations, is only limited by the time to select an aperture and upload it to the SLM. Since it is possible to preload shapes, switching could be done very rapidly. Figure 5 demonstrates the change in wall contrast that is obtained simply by collecting the scattered light at different orientations and these images could be further combined into one summation image to include all features obtained with the various apertures similar to the work of Rossi et al. [19] to improve RGC layer neuron visibility.

In addition to time efficiency, our detection scheme also enables more efficient use of light returned from the retina. By using the entire PSF, and directing the light to two, or potentially more, additional multiply scattered light views we have the same advantage of the split aperture approach, but now with the ability to optimize the orientation.

4.2 Optimizing conditions for retinal vasculature imaging

For smaller vessels imaged with a half annulus and fixed outer radius, it appears that the wall contrast of individual mural cells had a broad optimum for inner radii between 2.3 and 8.3 ADD. When the inner radius was larger, the contrast of the fine detail of the vessel wall structure diminished. Exact details seemed to depend on vessel orientation and retinal thickness (see below).

In contrast with Chui et al. [9], we often resolved the wall structure and laminar flow in venules (Fig. 2C and Fig. 2E). While decreasing the inner radius helps to capture the small scatter from the venule walls, the more specialized shape of the half annulus also likely improves the contrast of these and smaller structures as well. With a half annulus, more of the PSF center is removed compared with an offset aperture that is limited in its angular extent. Thus, we are more selectively capturing the scattered light with a half annulus and more background scatter is removed further improving the contrast of small vessel structures.

For the few larger vessels ($> 50\mu m$) imaged, varying the inner radius did not qualitatively have as large of an impact of viewing the vessel wall structure (Fig. 2E, F) as for smaller vessels. This difference in contrast could arise from the fact that larger vessels are generally located in regions where the retina is thicker compared to the smaller vessels that were the primary focus of this study. The thicker retina could enable those structures to scatter longer distances before a second scattering. As we were limited in the number of larger vessels imaged in this study, further investigation into optimal aperture parameters should be investigated for larger vessels and vessels located in thicker retina.

For vessels of all sizes, strong scatter from the erythrocytes moving through the vessel was evident even with large displacements of the half annulus from the center of the PSF. Even when both the inner and outer radii were displaced greatly (Fig. 4D), time varying scatter from the center of the vessels was still visualized although individual erythrocytes were not.
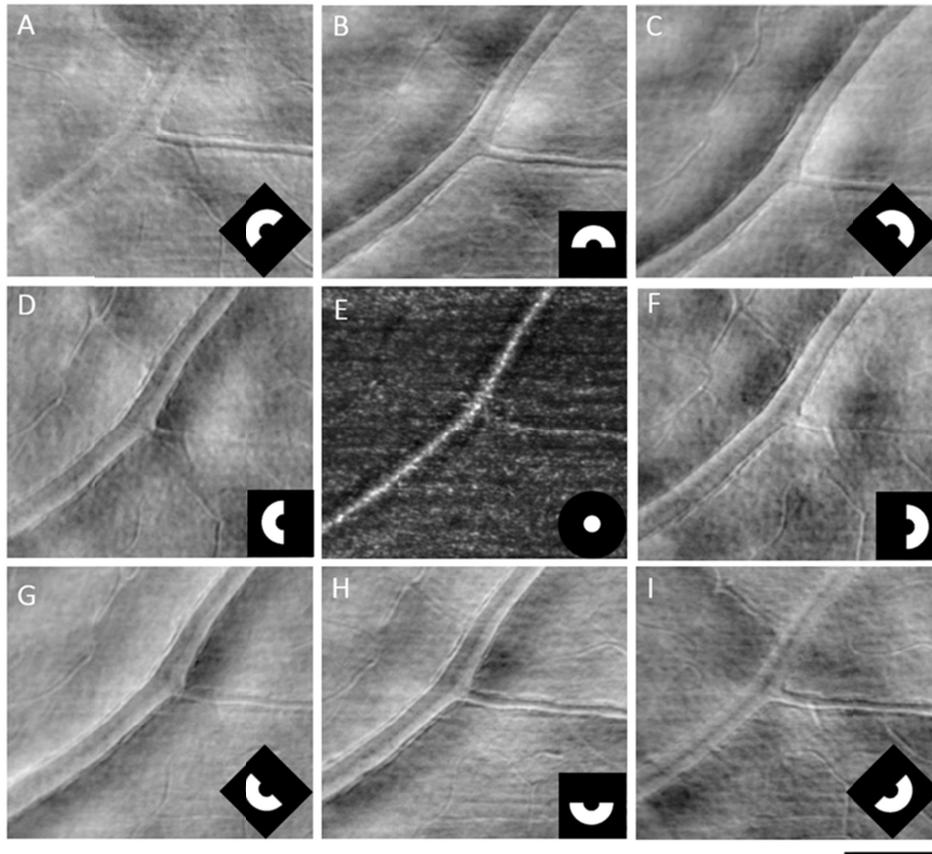

Fig. 5. Retinal feature contrast varies with split annulus orientation at a fixed inner and outer radius (8.3 ADD and 22.7 ADD) in a healthy 24 yo subject. Arteriole wall contrast of the parent vessel changed with the half annulus angle orientation (compare A and I vs C and G). An array of presumed ganglion cells are visible at all orientations and follow the orientation of the nerve fiber layer. The confocal image (E) is shown for comparison. Scale bar = 100 μm.

4.3 Other retinal structures visualized

Although the primary focus of this study was on imaging the retinal vasculature, other transparent cells, presumably RGC layer neurons were consistently identifiable when focused on the inner retina and utilizing the half annulus aperture on our SLM (Fig. 5). While we were often collecting scattered light in a similar range of displacements from the center of the PSF as Rossi et al[19], comparable contrast of the RGC layer neurons in our study was achieved with just one half annulus image (100 frames or less) and did not require combining contrast across images (Fig. 5). Similar to the venule walls, these low contrast cells may benefit from the decreased background light provided by a half annulus aperture.

While we focused primarily on half annulus and split detector configurations, additional apertures including an annulus, single quadrants, and dual quadrant configurations were also

successfully utilized. However, these data (not shown) did not further enhance imaging of the retinal vasculature although we did not explore the full range of possible parameters. In theory, any binary shape could be uploaded to the SLM and in the future, further specializing the aperture shape could enable better resolution or enhanced contrast of the structures presented here as well as other translucent bodies in the retina.

4.4 Limitations

While efficiency was improved using the electronic control of the SLM to change aperture parameters compared to conventional methods, we were still limited by the amount of time to enter the parameters into the GUI. However, since imaging for most features is not highly sensitive to most of the parameters, it is feasible to present the operator with a subset of pre-loaded conditions, chosen by mouse click to allow even more rapid interchange. When imaging a vessel with a half annulus, most vessels could be imaged with a fixed orientation, and when we were testing scattering distance by manipulating the half annulus parameters, we maintained a fixed orientation despite the vessels being at various orientations. Likewise, we used a half annulus of a fixed size with a moderate inner radius to investigate scattering direction by changing the orientation of the split annulus. It is possible that our parameter space did not include the optimal conditions for orientation and small distances and additional experiments could yield even better results.

As mentioned previously, the mirror flipping that our SLM goes through causes lines through the image that we removed computationally in post-processing. There are options for electronically suppressing these [26], as well as using more complex controller to avoid this problem.

Lastly, as we change aperture sizes, the amount of light directed to the "ON" and "OFF" detectors varies markedly. This required changing the voltage to the APD detectors between conditions. While reasonable presets for these voltages were used and are under computer control, we also need to better calibrate the gain changes to provide calibrated contrast values. We do keep the temperatures of the APD's controlled so gains are sufficiently stable to make this feasible.

5. Conclusions

An SLM placed at a retinal conjugate plane can effectively be used as a rapidly configurable aperture enabling efficient collection of multiply scattered light in various directions and distances of particular retinal features. The retinal microvascular network is complex in regards to vessel orientation and size. Utilizing an approach that automates through a series of configurations will be particularly useful when studying retinal vascular diseases such as diabetic retinopathy and understanding the changes that occur to the vessel wall structure.